NASA CR-
141699

Lockheed

HUNTSVILLE RESEARCH & ENGINEERING CENTER

LOCKHEED MISSILES & SPACE COMPANY

A GROUP DIVISION OF LOCKHEED AIRCRAFT CORPORATION

HUNTSVILLE, ALABAMA

48

TM 54/20-334
LMSC-HREC D2255

LOCKHEED MISSILES & SPACE COMPANY
HUNTSVILLE RESEARCH & ENGINEERING CENTER
HUNTSVILLE RESEARCH PARK
4800 BRADFORD DRIVE, HUNTSVILLE, ALABAMA

Analysis of the Experimental Space Shuttle Orbiter Plume Heating Rate Results Obtained in the GAC Detonation Tube Plume Simulator Facility

January 1972

Contract NAS8-11758

by

C. J. Wojciechowski
M. M. Penny

Juan K. Lovin, Supervisor
Thermal Environment Section

George D. Reny, Manager
Aeromechanics Dept.

FOREWORD

This document was prepared by personnel at the Lockheed-Huntsville Research & Engineering Center, Huntsville, Alabama, for the Manned Spacecraft Center, Houston, Texas. This report presents the results of a preliminary analytical study of the Grumman Aerospace Corporation experimental plume impingement heating rate results obtained in their Detonation Tube Plume Simulator Facility. This work was performed under Contract NAS9-11758, "Space Shuttle Plume Impingement Study," at the request of Mrs. I. H. Fossler, Flight Technology Branch, Manned Space Flight Center.

An experimental study of the plume impingement heating on the space shuttle booster afterbody resulting from the space shuttle orbiter engine plumes was conducted in the Grumman Aerospace Corporation's Detonation Tube Plume Simulator Facility. The 1/100-scale model tests consisted of one- and two-orbiter engine firings on a flat plate, a flat plate with a fin, and a cylinder model. The plume impingement heating rates on these surfaces were measured using thin film heat transfer gages. The detonation tube plume simulator flow field was calculated using an axisymmetric real gas method-of-characteristics computer program. The detonation tube plume simulator flowfield calculation was initiated at the nozzle throat using the gaseous products of combustion behind the detonation wave. For the two engines firing simultaneously the resulting plume flow field in the plume/plume interaction region was approximated using an axisymmetric single engine plume from an "equivalent" engine in which the overall mass flow and exit momentum are preserved.

In general overall good agreement was achieved between the analytical heating rate results and the test data for the flat plate and cylinder models for both the single and two-engine tests. The experimental heating rates on the vertical fin in the region near the top of the fin correlated well with laminar theory. The experimental heating rates on the vertical fin near the root correlated well with the laminar theory when the upstream interference flow from the flat plate was considered in the analysis. The heating rates on the fin in the region of the plume centerline were underpredicted. Several possible explanations for this underprediction are discussed in this report.

LIST OF TABLES AND ILLUSTRATIONS

CONTENTS (Continued)

NOMENCLATURE

Symbol

c_p	specific heat (Btu/slug-^oR)
g	gravitational constant (ft-lbf/lbm-sec^2)
g'(o)	enthalpy gradient
H	total enthalpy (Btu/slug)
h	static enthalpy (Btu/slug)
J	conversion factor 778 ft-lbf/Btu
M	Mach number
m	exponent used in Eq. (7)
O/F	oxidizer-to-fuel ratio
P	pressure (psf)
Pr	Prandtl number (dimensionless)
$\dot{q}$	convective heating rate (Btu/ft^2-sec)
r_e	nozzle exit radius
R	radius of curvature (ft)
r	recovery factor
S'	defined in text after Eq. (4)
s	streamline distance (ft)
T	temperature (^oR)
V	velocity (ft/sec)
X	flat plate equivalent length (ft)
x	distance from nozzle exit plane (ft)

Subscripts

e	boundary layer edge value
eff	effective
L	laminar value
r	boundary layer recovery value

NOMENCLATURE (Continued)

Subscripts

s	stagnation line value
T	turbulent value
w	wall value
∞	freestream value

Superscript

*	evaluated at Eckert Reference Enthalpy

Greek

α	impingement angle (radians)
γ	ratio of specific heats
ϵ	streamline divergence factor (ft)
μ	viscosity (slug/ft-sec)
ρ	density (slug/ft^3)

Section 1
INTRODUCTION

The study effort documented herein is part of an overall study effort to define the plume impingement environment on space shuttle booster surfaces subject to direct plume impingement from the orbiter main engines during the staging maneuver. As part of this study effort, comparisons of the analytical results with experimental data are made as the experimental data becomes available. An experimental study (Ref. 1) of the plume impingement heating on the space shuttle booster afterbody resulting from the space shuttle orbiter engine plumes was conducted in the Grumman Aerospace Corporation's (GAC) Detonation Tube Plume Simulator Facility. The 1/100-scale model tests consisted of one and two-orbiter engine firings on a flat plate, a flat plate with a fin, and a cylinder model. The plume impingement heating rates on these surfaces were measured using thin film heat transfer gages.

The analytical techniques used to define the detonation tube plume simulator flow field and the plume impingement heating rates are presented in Section 2. A discussion of the analytical results obtained and the comparisons with experimental data are presented in Section 3.

Section 2
TECHNICAL DISCUSSION

The experimental program described in Ref. 1 was conducted using a short-duration plume simulation technique specifically designed for the hydrogen-oxygen propellant system of future space shuttle engines. The nozzle contours of the future space shuttle engines were geometrically scaled (1/100-scale models). The tests consisted of one and two engines firing simultaneously on a flat plate, a flat plate with a fin, and a cylinder model. The analytical techniques used to calculate the resulting plume flow fields and impingement heating rates are presented in this section.

2.1 GAC DETONATION TUBE PLUME SIMULATOR

The plume properties used in the analytical plume impingement analysis were computed using the Lockheed-Huntsville Method-of-Characteristic (MOC) Computer Program (Refs. 2 and 3). Thermochemistry properties for the plume calculations were computed using the NASA-Lewis Chemical Equilibrium Combustion (CEC) Computer Program (Ref. 4). A description of these calculations is given in the following sections.

2.1.1 Thermochemistry Analysis

The thermochemistry properties of the nozzle-plume flow field were computed assuming the flow to be in thermal equilibrium. Initial state conditions for the nozzle were computed using the Chapman-Jouguet detonation option of the CEC program. Thermochemistry data for use in the MOC program were then obtained by computing the flow expansion properties from the reference condition. These properties are tabulated in Table 1 as functions of the local Mach number with the local specie concentrations tabulated in Table 2.

An investigation was conducted to determine if at the test operating conditions any deviations from the equation of state for a thermally perfect gas would occur for the gas mixture. A previous study (Ref. 5) examined a range of combustion conditions applicable to the space shuttle vehicle. Deviations from the computed perfect gas thermodynamic values for pressure values less than 300 atm were found to be small for the real gas analysis. It was concluded, therefore, that the thermally perfect gas assumptions used to calculate the gas thermodynamic properties could be employed for the test conditions.

2.1.2 Nozzle-Plume Flowfield Analysis

A detailed analysis of the nozzle-plume flow field was performed. Real gas effects were accounted for in the thermochemistry analysis, and the nozzle shock wave was also considered throughout the flowfield calculations. Table 3 presents the nozzle contour coordinates.

In the analysis the flow was assumed to be inviscid and axially symmetric. A previous study (Ref. 6) has shown that during the flow expansion through the nozzle the products of combustion of hydrogen and oxygen are very stable and approach a chemically frozen condition just downstream of the nozzle throat. In the present case the primary constituents are H_2O and H_2 (Table 2). For Mach numbers greater than 4.39 the global molecular weight is constant (14.112) and the flow is essentially chemically frozen. The isentropic exponent, gamma, then becomes a function only of temperature. Those regions of the plume flow field having Mach numbers greater than 7.729 (Table 1) were treated as an ideal gas at a molecular weight of 14.112 and an isentropic exponent of 1.3131. This results from the fact that thermochemical data are not available to the program for conditions above that Mach number.

The nozzle flowfield solution was initiated at the geometric throat with a straight start line using a Mach number of 1.01. In the nozzle flow field a shock wave is formed as a result of a discontinuity in slope at the junction of the throat and nozzle surface. This shock wave intersects the nozzle-plume axis approximately 1.5 nozzle radii downstream of the nozzle exit plane.

The plume boundary at the nozzle lip was generated for the nozzle flow expanding to a back pressure of 5×10^{-5} torr.

The plume flowfield properties are shown in Figs. 1 through 6. Figure 1 shows the percent distribution of mass flow in the plume flow. The axial, x, and radial, r, coordinates are measured with respect to the nozzle exit plane. The local property values have been made nondimensional with respect to the nozzle reference conditions (Table 1) with the data presentation in terms of contour maps of the respective property.

The flow field in the vicinity of the nozzle lip and along the plume boundary is a region of expanding high-speed flow. The characteristic lines in this region become parallel and approach the streamline asymptotically. (The Mach angle approaches 0.0 as the Mach number approaches infinity.) Due to the extremely high Mach numbers, the characteristic lines become divergent in the outer regions of the lip expansion fan and along the plume boundary. Consequently, portions of the outermost regions of the plume flow field were not calculated. This region amounts to less than 1% of the calculated mass flow and should have no significant consequence in applying the calculated plume to the plume impingement analysis.

The presence of the shock wave (which is of variable strength and locally strong in the vicinity of the axis but very weak in the plume far away from the nozzle exit plane) is responsible for a gradient in entropy across those regions of the flow field downstream of the shock waves. Therefore, lines of constant Mach number are not lines of constant pressure.

Knudsen number calculations were made at various points in the plume to determine if the flow was in the non-continuum flow regime. Temperature gradients indicate the flow is completely within the continuum flow regime over the region of interest.

2.2 PLUME IMPINGEMENT HEATING ANALYSIS

The analytical plume impingement heating rates used in the analytical/data comparisons were computed using the Lockheed-Plume Impingement Computer Program (Refs. 7 and 8). Calculations of the local plume Knudsen numbers indicated that only the continuum flow regime was encountered for this study. Several different semi-empirical heat transfer theories were used to calculate the heating rates on the various surfaces for the GAC tests and will be described as a function of the various impinged surfaces.

2.2.1 Cylinder and Vertical Fin Heat Transfer Theory

For the cylinder tests, heat transfer rate calculations were made for both laminar and turbulent boundary layers. For analytical purposes, the impingement flow field on the cylinder and fin was assumed to be characterized by the formation of a stagnation line streamline down the body and chordwise streamlines around the body as shown in the following sketch.

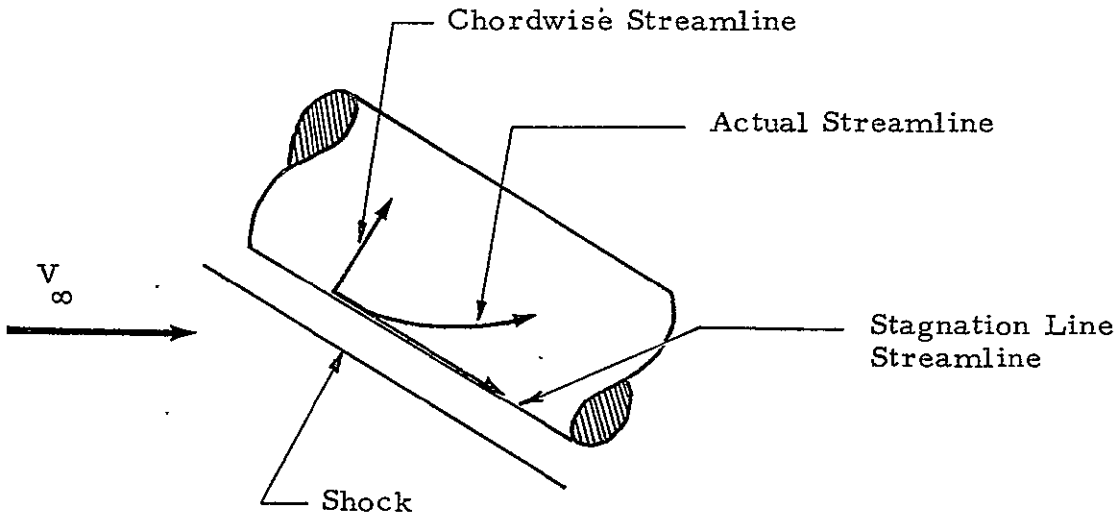

Along the stagnation lines the following theories were used.

- Laminar Stagnation Line

The heat transfer rates along the stagnation line for a laminar boundary layer was calculated using the semi-empirical correlations of Refs. 9 and 10. The resulting heat transfer correlation used was:

$$\dot{q}_s = \frac{0.565}{Pr_w^{0.6}} \sqrt{\rho_w \mu_w \frac{dV}{dR}} \left(\frac{\rho_e \mu_e}{\rho_w \mu_w}\right)^{0.44} (H_r - h_w). \qquad (1)$$

The method used to calculate the gas transport properties is based on the Lennard-Jones potential intermolecular force model as discussed in detail in Ref. 7.

When the impinged body is small compared to the impinging plume flow field as is the case for the vertical fin, the velocity gradient can be estimated by combining the Bernoulli equation along the boundary edge in the chordwise direction with the Newtonian pressure distribution, i.e.,

$$\frac{dV}{dR} = \frac{1}{R} \sqrt{2g \left(\frac{P_s - P_\infty}{\rho_s}\right)} \qquad (2)$$

If the freestream velocity component is subsonic, then as pointed out in Ref. 11 the velocity gradient will be underpredicted using Eq.(2). In this case, the velocity gradient is calculated using the following equation from Ref. 11, i.e.,

$$\frac{dV}{dR} = \frac{2 V_\infty \sin\alpha}{R} \left[1 - 0.416 (M_\infty \sin\alpha)^2 - 0.164 (M_\infty \sin\alpha)^4\right] . \qquad (3)$$

When the impinged body is large compared to the impinging plume flow field, as is the case for the cylinder, then the velocity gradient is calculated based on the pressure gradients in the chordwise direction (Ref. 12). In this case, the radius parameter appearing in Eq. (2) is replaced by an effective radius of curvature (R_{eff}) which is calculated using the experimental results of Ref. 13. The effective radius of curvature is,

$$R_{eff} = \frac{S'}{0.225} , \tag{4}$$

where S' is the surface distance from the stagnation point to the point on the body where the surface impact pressure (P) has decayed to $0.95 P_s$. This is shown in the following sketch.

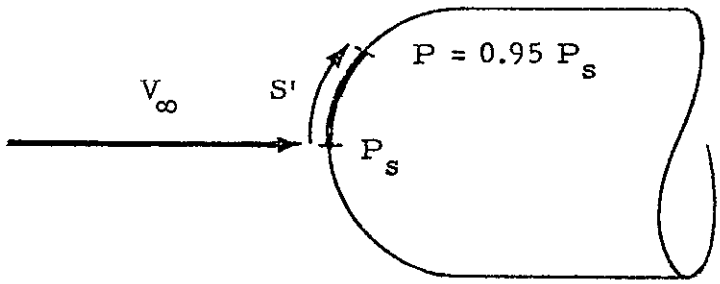

Using Eq. (4), values for R_{eff} were calculated for the family of blunt bodies documented in Ref. 14 and the results obtained agreed within 10% of the published results in Ref. 14.

- Turbulent Stagnation Line

The heat transfer rate along the stagnation line for a turbulent boundary layer is calculated using a modified version of the turbulent swept cylinder theory of Beckwith and Gallagher (Ref. 15), i.e.,

$$\dot{q}_s = \frac{0.0288}{Pr_w} \left(\frac{V_\infty \cos\alpha}{\mu_s} \right)^{0.6} \left(\frac{dV}{dR} \right)^{0.2} (\rho_w \mu_w)^{0.8} (H_r - h_w) . \qquad (5)$$

Modifications to this theory include the introduction of the enthalpy driving potential to make it more applicable to boundary layers in plumes. The complete derivation of Eq. (5) is given in Ref. 15. Briefly, the integral energy and momentum equations for the turbulent boundary layer on a yawed infinite cylinder are solved using simplifying assumptions for skin friction, velocity and thermal profiles, secondary flow and Reynolds analogy. Equation (5) is based on the assumption of a Blasius flat plate skin-friction law for the flow along the leading edge and zero secondary flow which is valid only at the stagnation line.

The velocity gradient can be estimated from Newtonian theory or from the calculated pressure gradients in the stagnation region as discussed previously, i.e., Eqs. (2) or (3) or (4).

- Heat Transfer Distributions Off the Stagnation Line

Equations (1) and (5) are valid only along the flow stagnation lines. To obtain heat transfer distributions off the stagnation lines use is made of semi-empirical correlations.

Laminar Flow: The heating rate at a point on the surface for an isothermal wall with local similarity assumed can be expressed in terms of the heat transfer rate at the stagnation line by,

$$\frac{\dot{q}}{\dot{q}_s} = \frac{\left(\frac{P}{P_s} \right) \left(\frac{V_e}{V_\infty} \right)}{\sqrt{2 \int_o^s \left(\frac{P}{P_s} \right) \left(\frac{V_e}{V_\infty} \right) ds \, \frac{1}{V_\infty} \frac{dV}{dR}}} \left[\frac{g'(0)}{g'_s(0)} \right] \qquad (6)$$

The preceding equation consists of the product of inviscid and viscous quantities. The inviscid quantities require a knowledge of the local surface pressure distribution as well as the thermodynamics of the inviscid flow. The viscous quantities, i.e., $g'(0)$ and $g'_s(0)$, require the appropriate solution to the boundary-layer equations which are implicitly related to the inviscid flow through the local surface pressure and pressure gradient. The preceding statement infers that the heating rate ratio given in Eq. (6) is dependent on the pressure ratio, i.e.,

$$\frac{\dot{q}}{\dot{q}_s} = \left(\frac{P}{P_s}\right)^m \quad . \tag{7}$$

Available data indicate that on hemispherical forebodies the exponent m in Eq. (7) assumes values between 0.8 and 0.9 while over the afterbody, m assumes values between 0.9 and 1.0. These results demonstrated the strong dependence of heating rate ratio on pressure ratio and are useful for reasonable estimates of the local heating rates once the stagnation line heating rates are known. Examination of heating rate ratios for yawed cylinders revealed the same dependence of heating rate ratio on pressure ratio. The value of m in Eq. (7) which correlated the heating rate ratio best was a value of 0.85. Due to the simplicity and speed (short computation time) afforded through the use of Eq. (7), this equation is used in the plume impingement program to obtain heating rates off the stagnation lines.

Turbulent Flow: The heating rates off the stagnation lines for turbulent flow are calculated using a modified form of the heat transfer ratio derived in Ref. 15, i.e.,

$$\frac{\dot{q}}{\dot{q}_s} = \left(\frac{P}{P_s}\right)^{\frac{3\gamma - 1}{2\gamma}} \left[\frac{\left(\frac{P_s}{P}\right)^{\frac{\gamma - 1}{\gamma}} - \frac{T_s}{T_o}}{1 - \frac{T_s}{T_o}} \right]^{0.375} \quad . \tag{8}$$

Examination of turbulent heating rate distribution data for yawed cylinders revealed that Eq. (8) correlated the data better than the original form of the equation presented in Ref. 15.

2.2.2 Flat Plate Heat Transfer Theory

For the flat plate tests, heat transfer rate calculations were made for both laminar and turbulent boundary layers. The boundary layer heat transfer theories used in the plume impingement computer program for flat plates are presented here.

- Laminar Flat Plate Convective Heat Transfer

Heat transfer through a laminar boundary layer is calculated using the integral form of the energy equation. Effects of variable freestream velocity, density, and pressure are accounted for through use of appropriate transforms of the flat plate solution. Non-constant properties are also accounted for through the boundary layer.

Based on examination of several "exact" laminar boundary layer solutions, Eckert (Ref. 16) recommends that the effects of variable gas properties through the boundary layer can be accounted for by simply evaluating the properties at a "reference enthalpy" and using these values in the constant property solutions as obtained by Blasius. Based on this method, the convective heat rate to the wall is evaluated using,

$$\dot{q} = \frac{0.332}{Pr^{*\,2/3}} \cdot \frac{(\rho^* \mu^* V_e)^{0.5}}{X_L^{0.5}} (H_r - h_w) . \qquad (9)$$

The recovery enthalpy is evaluated by

$$H_r = \int_o^{T_e} c_p \, dT + \frac{r V_e^2}{2J} , \qquad (10)$$

where

$$r = \sqrt{Pr^*} \tag{11}$$

The starred (*) properties in Eq. (9) refer to properties evaluated at a temperature corresponding to a "reference enthalpy," h*, where

$$h^* = h_e + 0.5\,(H_s - h_e) + 0.22\,(H_r - h_e). \tag{12}$$

The characteristic length (X_L) as used in Eq. (9) is obtained for variable property flow by numerically integrating the following equation along a flowfield streamline, (Refs. 17 and 18)

$$X_L = \frac{1}{\rho^* \mu^* V_e \epsilon^2} \int_o^s \rho^* \mu^* V_e \epsilon^2 \, ds. \tag{13}$$

The parameter s is the wetted length along the streamline. The parameter ϵ accounts for the divergence of the streamlines due to crossflow pressure gradients. Presently the PLIMP program (Ref. 8) does not calculate this streamline divergence but it is planned to add this capability in the near future. At present, for a flat plate, the parameter ϵ is set equal to 1.0 and thereby divided out.

In the initial plume impingement region on a flat plate, the streamline distance (X_L) in Eq. (9) approaches zero and the heating rate would theoretically approach infinity. In the initial impingement region, heating rates can be approximated by utilizing Eq. (1) with the velocity gradient calculated using Eqs. (2) and (4).

- Turbulent Flat Plate Convective Heat Transfer

A similar method of analysis is used for calculating heating rates from a turbulent boundary layer as for the laminar boundary layer just discussed. For a turbulent boundary layer, the convective heating rate to the wall was evaluated using,

$$\dot{q} = \frac{0.0296}{Pr^{*.66}} (\rho^* V_e)^{0.8} \left(\frac{\mu^*}{X_T}\right)^{0.2} (H_r - h_w). \tag{14}$$

The starred parameters density, viscosity and Prandtl number are again calculated at a reference temperature corresponding to the Eckert reference enthalpy Eq. (12). The Eckert reference enthalpy is calculated as in the laminar case except that the recovery factor, r, is

$$r = Pr^{*\,1/3} \tag{15}$$

The recovery enthalpy is calculated using Eq. (10).

The characteristic length, X_T is defined (Ref. 19) by

$$X_T = \frac{1}{\rho^* \mu^* V_e \epsilon^{1.25}} \int_o^s \rho^* \mu^* V_e \epsilon^{1.25}\, ds, \tag{16}$$

where s is the distance along the streamline.

For a flat plate, the parameter ϵ is presently set equal to a constant in the PLIMP program (Ref. 8) and thereby divided out.

Section 3
DISCUSSION OF RESULTS

In this section comparisons are made between the theoretical results obtained using the techniques presented in Section 2 and the GAC experimental data. For the two-engine firings, the resulting three-dimensional plume flow field was treated analytically using an axisymmetric single engine plume flow field from an "equivalent" engine in which the overall mass flow and exit momentum are preserved.

3.1 FLAT PLATE RESULTS

The flat plate test model is shown in Fig. 7. Figure 8 shows the experimental and analytical heating rate distributions on the flat plate along the engine centerline (Row C) for the single-engine firing. The increase in heating in the analytical results at the x/r_e value of 10.5 is due to the nozzle internal shock impinging on the flat plate in this region (refer to Fig. 6). The analytical increase in heating shown in Fig. 8 due to the nozzle internal shock is the result of local property variations across the shock as used in Eqs. (9) and (14). Unfortunately, the heat transfer gages on the flat plate were spaced too far apart to measure the exact location of the impingement of the nozzle internal shock on the flat plate. However, the trend of the test data shown in Fig. 8 exhibits a plateau in the region between $x/r_e = 12$ and $x/r_e = 15$ indicating the presence of an impinging shock in this region. This region is farther downstream than the $x/r_e = 10.5$ location indicated by the analytical results. The reason for this difference is because, in this preliminary analysis, the intersection of the nozzle internal shock with the plume impingement shock off the flat plate was not treated in the impingement flowfield analysis. Due to this shock intersection in the flow field, the nozzle internal shock would be deflected and would impinge on the flat plate farther downstream than the $x/r_e = 10.5$ location and would be in better agreement with the indicated test results.

In the initial impingement region, i.e., from x/r_e = 3 to 5, the dashed line shown in Fig. 8 indicates the laminar flat plate results obtained using Eq. (9). The solid laminar line in this region was obtained using the laminar swept cylinder theory (Eq. (1)) with the effective radius of curvature determined by Eq. (4).

Since the flat plate theory used considered only streamwise pressure gradients and not crossflow pressure gradients which would cause divergence of the streamlines, it is expected that the theories would underpredict the data in the region where large crossflow pressure gradients exist, i.e., in the region between x/r_e = 6 to x/r_e = 18. Therefore, since overall good agreement is indicated in Fig. 8 between the test data and the turbulent results it should not be concluded that the boundary layer is turbulent. It is planned in the near future to add the capability to the plume impingement program which will calculate the effects due to crossflow pressure gradients. The local Reynolds number based on running length and the local momentum thickness Reynolds number are plotted in Fig. 9 for Row C. The momentum thickness used in the momentum thickness Reynolds number calculation was based on the equivalent flat plate length as defined by Eq. (13).

Figure 10 shows the experimental and analytical heating rate distributions on the centerline of the flat plate (Row B) for the single engine firing. The trends shown in this figure are similar to the trends shown in Fig. 8.

Figure 11 shows the experimental and analytical heating rate distributions on the centerline of the flat plate (Row B) for two engines firing. The analytical results denoted by the solid lines were obtained using an "equivalent" multiple engine plume. The analytical results denoted by the dashed lines were obtained using a more "exact" definition of the three-dimensional plume flow field. These results were obtained by first inserting a vertical plate between the two engines and calculating the resulting local flow velocity, direction, and entropy on the vertical plate using tangent wedge theory. The resulting flow properties on the vertical plate along the intersection line of this vertical plate

and the test plate were then used to calculate the heating rates along Row B on the test plate. In comparing the two analytical results presented in Fig. 11 it can be seen that the "equivalent" engine method does appear to yield satisfactory results except for the initial plume impingement region, i.e., for values of x/r_e less than 6. The local Reynolds number based on running length and the local momentum thickness Reynolds numbers along Row B are plotted in Fig. 12 for the two-engine firing. The momentum thickness used in the momentum thickness Reynolds number calculation was based on the equivalent flat plate length as defined by Eq. (13).

Figure 13 shows the experimental and analytical heating rate distributions on the outboard line (Row A) of the flat plate. The analytical results denoted by the solid lines are for the single engine firing and compare favorably with the single engine test data. In this case, the single engine that was firing was the engine with its centerline located along Row C on the flat plate (Fig. 7). The analytical results denoted by the dashed lines are for the two engines firing and were obtained using the "equivalent" engine plume. Examination of glow photographs taken during the test reveals that the plume/plume interaction shock would cross Row A on the flat plate at approximately an $x/r_e \sim 14$. The single-engine and two-engine data are approximately the same level at an $x/r_e = 9$. At an $x/r_e = 15$, the two-engine data show a large rise indicating that this point is within the two-plume interaction region.

3.2 CYLINDER RESULTS

The cylinder test model is shown in Fig. 7. The experimental and analytical heating rate distributions on the cylinder along Row B for the single engine and two-engine firings are shown in Fig. 14. The analytical results presented were calculated using the yawed infinite cylinder equations, i.e., either Eq. (1) or (5), with the effective radius of curvature as defined by Eq. (4). In general, overall good agreement is shown between the test data and the laminar yawed infinite cylinder theory. The analytical results for the two-engine firing were calculated using the "equivalent" engine plume. Figure 15 shows the experimental and analytical heating rate distributions on the cylinder along Row E

for the single and two-engine firings. In general, overall good agreement is again shown between the test data and the laminar yawed infinite cylinder theory for the single and two-engine firing tests.

3.3 VERTICAL FIN RESULTS

On the flat plate test model, a vertical fin was mounted as shown in Fig. 16. The base of the vertical fin was located 9.21 exit radii downstream of the exit plane and had a leading edge radius of 0.125 inches. The experimental and analytical heating rate distributions along the fin leading edge are shown in Fig. 17 for two-engines firing. The experimental heating rates on the vertical fin in the region near the top of the fin correlate well with the laminar swept infinite cylinder theory. In the other regions on the fin the laminar swept infinite cylinder theory substantially underpredicts the experimental data. Bushnell, in Ref. 20, investigated the interference heating on a swept cylinder in the region of its intersection with a flat plate. Using the technique presented in Ref. 20, the interference heating on the vertical fin near the root was calculated for this test. The method used was to calculate the inviscid flowfield properties on the flat plate ahead of the vertical fin and to use these flow conditions in the yawed cylinder heating rate equations. The results obtained are noted in Fig. 17. Figure 18 is a sketch of the plume flowfield shock structure ahead of the vertical fin. The shaded area in the flow field ahead of the vertical fin is the flowfield interaction region between the two engines due to the nozzle internal shocks. This is the region where disagreement exists between the data and the analytical results. Higher plume static pressures will exist in this region of the flow field compared to the "equivalent" engine plume which was used in the calculations which could account for the disagreement noted. In addition, it is possible that this region could contain turbulence generated by the shock intersection upstream. Analysis conducted by Weeks in Ref. 21 indicate that a freestream turbulence level of approximately 9% can result in a measured heating rate being 2.25 times the predicted laminar value for the stagnation line on a cylinder. Another possible reason for the disagreement between the analytical and experimental results, is that the heating rate gages on the vertical fin in the region near

the plume centerline showed signs of particle impingement (Ref. 22). Particle impingement heating rates can be many times greater than the convective heating rates and this phenomenon alone could account for the discrepancy between the analytical and experimental results. Future tests are planned for the GAC Detonation Tube Facility which will include investigation into the reasons for the discrepancy between data and theory.

Section 4
CONCLUSIONS

Local heat transfer rates on simulated space shuttle booster surfaces due to space shuttle orbiter plume impingement were measured in the GAC 1/100-scale model tests. Using established plume impingement programs developed in support of NASA-MSFC and NASA-MSC plume impingement studies, the analytical heating rates for the 1/100-scale model tests were calculated. In general, overall good agreement was achieved between the analytical heating rate results and the test data for the flat plate and cylinder models. The experimental heating rates on the vertical fin in the region near the top of the fin correlated well with laminar swept cylinder theory. The experimental heating rates on the vertical fin near the root correlated better with the laminar theory when the upstream interference flow from the flat plate was considered in the analysis. However, the heating rates on the fin in the region near the plume centerline were underpredicted. Possible explanations which were discussed in this report for the underprediction are (1) particle impingement heating effects and (2) localized plume flowfield phenomena.

In order to apply scale model heat transfer test data to full-scale vehicles, one has to utilize the heat transfer scaling laws. When using the scaling laws, uncertainties arise as to which law to use depending on the nature of the boundary layer on the model on which the heat transfer data were obtained and on the full-scale vehicle. Based on the comparisons made in this report it is concluded that the boundary layer was laminar for the cylinder tests and probably laminar for the flat plate tests. The heat transfer data on the vertical fin was subject to local flowfield anomalies and would be difficult to scale to the full size vehicle. In the proposed future tests to be conducted in the GAC Detonation

Tube Facility it is planned to increase the plume Reynolds numbers gradually to match as closely as possible the full-scale vehicle Reynolds numbers. These future tests should yield useful information concerning boundary layer transition in rocket plumes.

REFERENCES

1. Jarvis, Leng, C. W. Osonitsch, and W. L. Konopka, "Experimental Study of Plume Impingement Heating from Orbiter Main Engines," GAC 552-1200 RD-31, Grumman Aerospace Corp., Bethpage, N. Y., May 1971.

2. Prozan, R. J., "Development of a Method-of-Characteristics Solution for the Supersonic Flow of an Ideal, Frozen, or Equilibrium Reacting Gas Mixture," LMSC-HREC D162220-III, Lockheed Missiles & Space Company, Huntsville, Ala., May 1970.

3. Smith, S. D., and A. W. Ratliff, "User's Manual — Variable O/F Method-of-Characteristics Program for Nozzles and Plume Flow Analysis," LMSC-HREC D162220-I, Lockheed Missiles & Space Company, Huntsville, Ala., May 1970.

4. McBride, Bonnie, and S. Gordon, "Preliminary Description of CEC, a Computer Program for Calculation of Chemical Equilibrium Composition with Applications," NASA-Lewis Research Center, Cleveland, Ohio, May 1969.

5. Audeh, Beverly, "A Preliminary Evaluation of Real Gas Effects at High Pressures and Temperatures for Space Shuttle Engines," LMSC-HREC D162312, Lockheed Missiles & Space Company, Huntsville, Ala., May 1970.

6. Penny, M. M., and S. D. Smith, "Definition of a Plume Flow Field with and Without External Nozzle Shock Wave of a Scaled J-2 Engine Operating at High Altitude Conditions," LMSC-HREC D148960, TN 54/20-58, Lockheed Missiles & Space Company, Huntsville, Ala., July 1971.

7. Wojciechowski, C. J., M. M. Penny, "Development of a High Altitude Plume Impingement Analysis for Calculating Heating Rates, Forces and Moments," LMSC-HREC D162867-I, Lockheed Missiles & Space Company, Huntsville, Ala., March 1971.

8. Penny, M. M., and C. J. Wojciechowski, "User's Manual and Description of a Computer Program for Calculating Heating Rates, Forces, and Moments Acting on Bodies Immersed in Rocket Exhaust Plumes," LMSC-HREC D162867-2, Lockheed Missiles & Space Company, Huntsville, Ala., March 1971.

9. Kemp, H. H., P. H. Rose, and R. W. Detra, "Laminar Heat Transfer Around Blunt Bodies in Dissociated Air," J. Aeron. Sci., 1959.

10. Beckwith, I. E., "Similar Solutions for the Compressible Boundary Layer on a Yawed Cylinder with Transportation Cooling," NASA TR R-42, 1959.

11. Reshotko, Eli, Ivan E. Beckwith, "Compressible Laminar Boundary Layer over a Yawed Infinite Cylinder with Heat Transfer and Arbitrary Prandtl Number," NACA Report 1379.

12. Wojciechowski, C. J., and R. J. Rader, "A Method for Calculating Stagnation Region Convective Heat Transfer to Arbitrary Surfaces Immersed in the Space Shuttle Attitude Control System Plumes," LMSC-HREC D162334, Lockheed Missiles & Space Company, Huntsville, Ala., May 1970.

13. Boison, J. C., and H. A. Curtiss, "An Experimental Investigation of Blunt Body Stagnation Point Velocity Gradient," ARS J., Vol. 29, No. 2, February 1959, pp. 130-135.

14. Ellison, James C., "Experimental Stagnation-Point Velocity Gradients and Heat-Transfer Coefficients for a Family of Blunt Bodies at Mach 8 and Angles of Attack," NASA TN D-5121, April 1969.

15. Beckwith, I. E., and J. Gallagher, "Local Heat Transfer and Recovery Temperatures on a Yawed Cylinder at a Mach Number of 4.15 and High Reynolds Numbers," NASA TR R-104, 1961.

16. Eckert, E. R. G., "Engineering Relations for Friction and Heat Transfer to Surfaces in High Velocity Flow," J. Aerospace Sci., August 1955, pp. 585-587.

17. Kays, W. M., Convective Heat and Mass Transfer, Chap. 14, McGraw-Hill, New York, N. Y., 1966.

18. Vaglio-Laurin, R., "Laminar Heat Transfer on Blunt-Nosed Bodies in Three-Dimensional Hypersonic Flow," WADC TN 58-147, Wright-Patterson AFB, Ohio, May 1958.

19. Vaglio-Laurin, R., "Turbulent Heat Transfer on Blunt-Nosed Bodies in Two-Dimensional and General Three-Dimensional Hypersonic Flow," J. Aerospace Sci., January 1960.

20. Bushnell, D. M., "Interference Heating on a Swept Cylinder in Region of Intersection with a Wedge at Mach Number 8," NASA TN D-3094, December 1965.

21. Weeks, Thomas M., "Influence of Freestream Turbulence on Hypersonic Stagnation Zone Heating," AFFDL-TR-67-195, Wright-Patterson AFB, Ohio, May 1968.

22. Telephone conversations between C. J. Wojciechowski (Lockheed-Huntsville), and Mr. Harold B. Hopkins, Grumman Aerospace Corporation, 19 January 1972.

Table 1

TABULATED VALUES OF THE PLUME THERMODYNAMIC PROPERTIES

O/F Ratio	M	M_w (lbm/lb_{mole})	γ	T (^oK)	P (atm)
6.	.000	12.708	1.13831	3810.00	68.045699
	1.000	12.899	1.13477	3620.80	39.299875
	1.770	13.254	1.13048	3286.69	13.609140
	2.161	13.468	1.13018	3083.72	6.804570
	3.262	13.994	1.16066	2414.91	.680457
	4.021	14.103	1.21044	1891.10	.136091
	4.391	14.110	1.22578	1670.92	.068046
	5.361	14.112	1.25520	1223.36	.013609
	5.821	14.113	1.26901	1062.55	.006805
	7.037	14.112	1.30008	753.13	.001361
	7.720	14.112	1.31307	631.28	.000680

Table 2

SPECIE CONCENTRATIONS AT THE REFERENCE AND PLUME FLOW CONDITIONS

Reference Conditions Mole Fractions (all gaseous)					
H	H_2	H_2O	O	OH	O_2
0.06937	0.26064	0.56372	0.01262	0.08285	0.01073
Mole Fractions in Plume (all gaseous)					
	H_2	H_2O			
	0.24399	0.75601			

Table 3

MODEL NOZZLE COORDINATES
(from Ref. 6)

X (in.)	R (in.)
-0.1153	.0865
0.0000	.0555
0.1523	.1386
0.3150	.2355
0.4448	.2982
0.5938	.3595
0.7496	.4145
0.9107	.4640
1.1000	.5144
1.2842	.5569
1.4900	.5981
1.5945	.6169
1.7004	.6346
1.8063	.6509
1.9126	.6663
2.0183	.6804
2.1237	.6935
2.2280	.7055
2.3606	.7195

Throat radius of curvature: 0.0588 in.

Exit plane lip angle: 5.75 deg

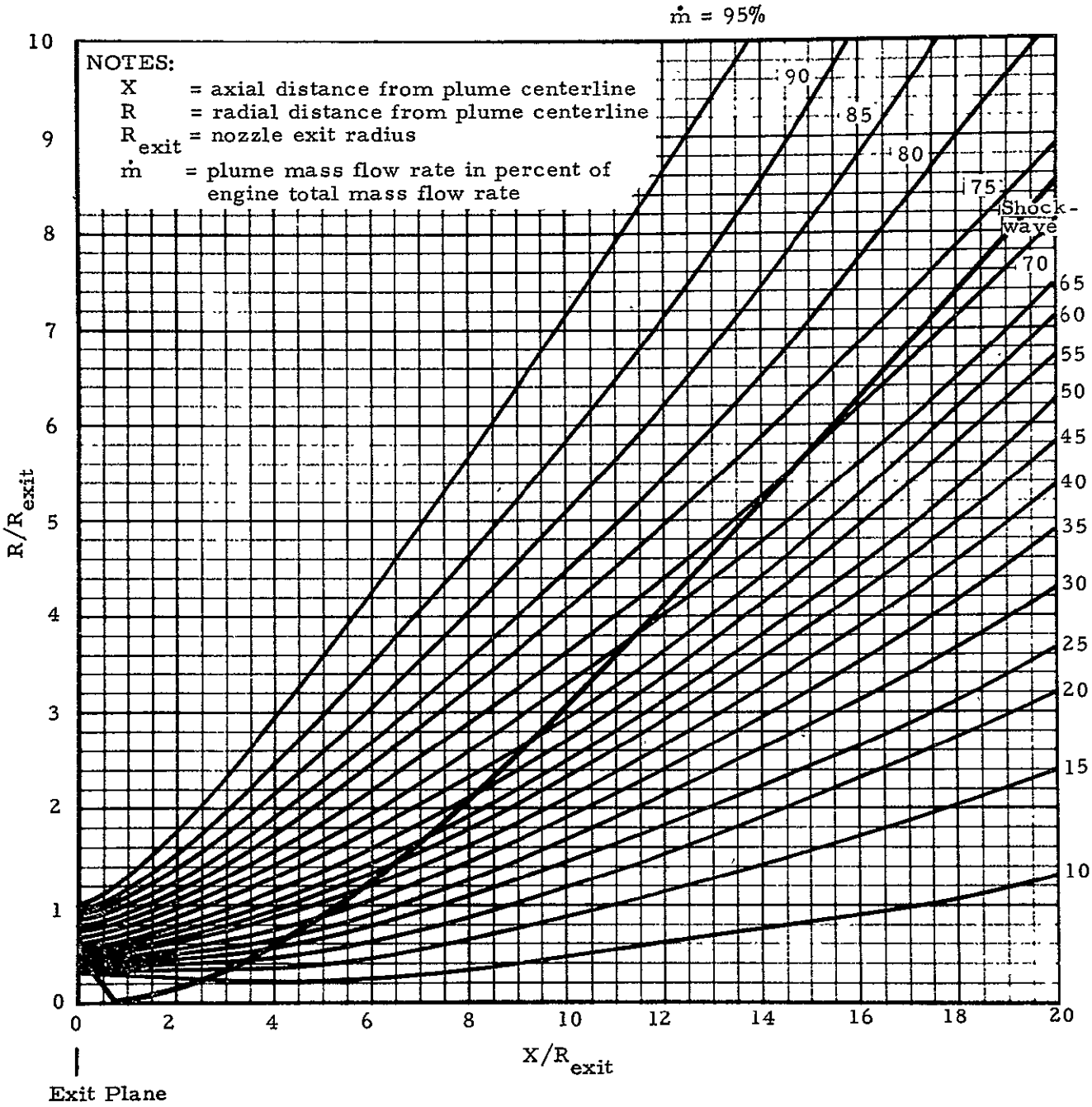

Fig. 1 - Distribution of Mass Flow Rate in the Engine Exhaust Plume

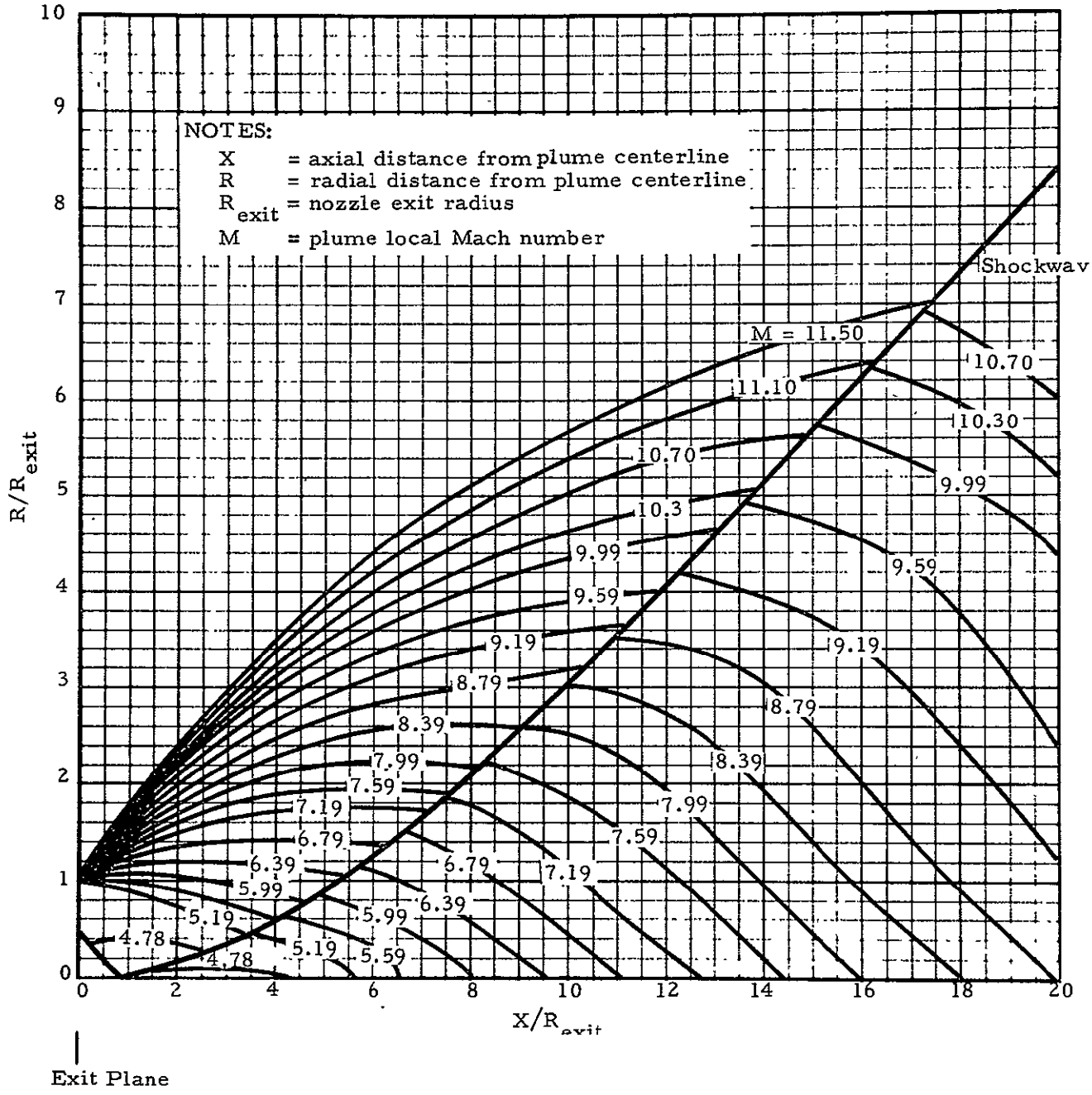

Fig. 2 - Local Mach Number Contour Map in the Engine Exhaust Plume

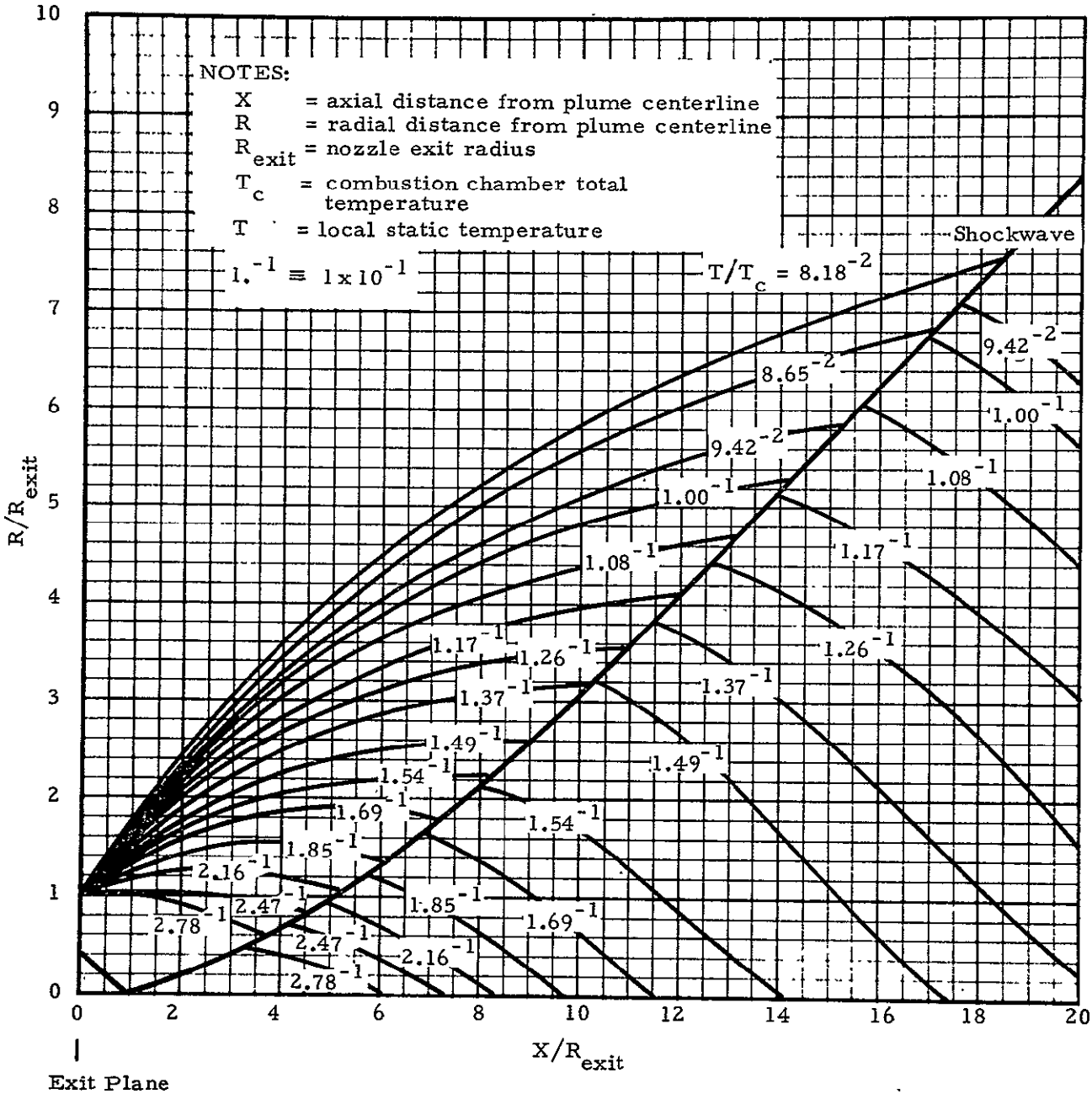

Fig. 3 - Local Static Temperature Contour Map for the Engine Exhaust Plume

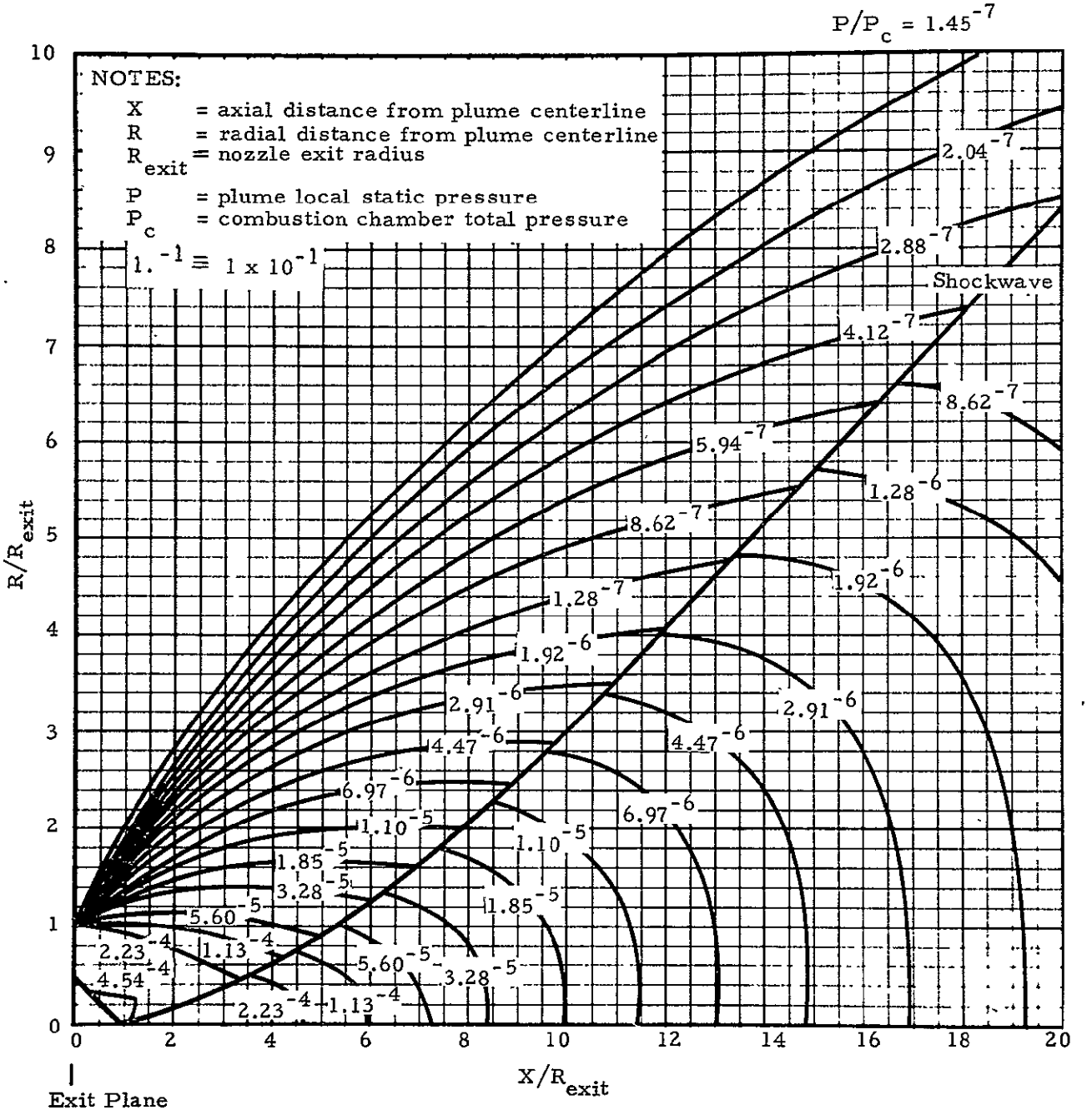

Fig. 4 - Local Static Pressure Contour Map for the Engine Exhaust Plume

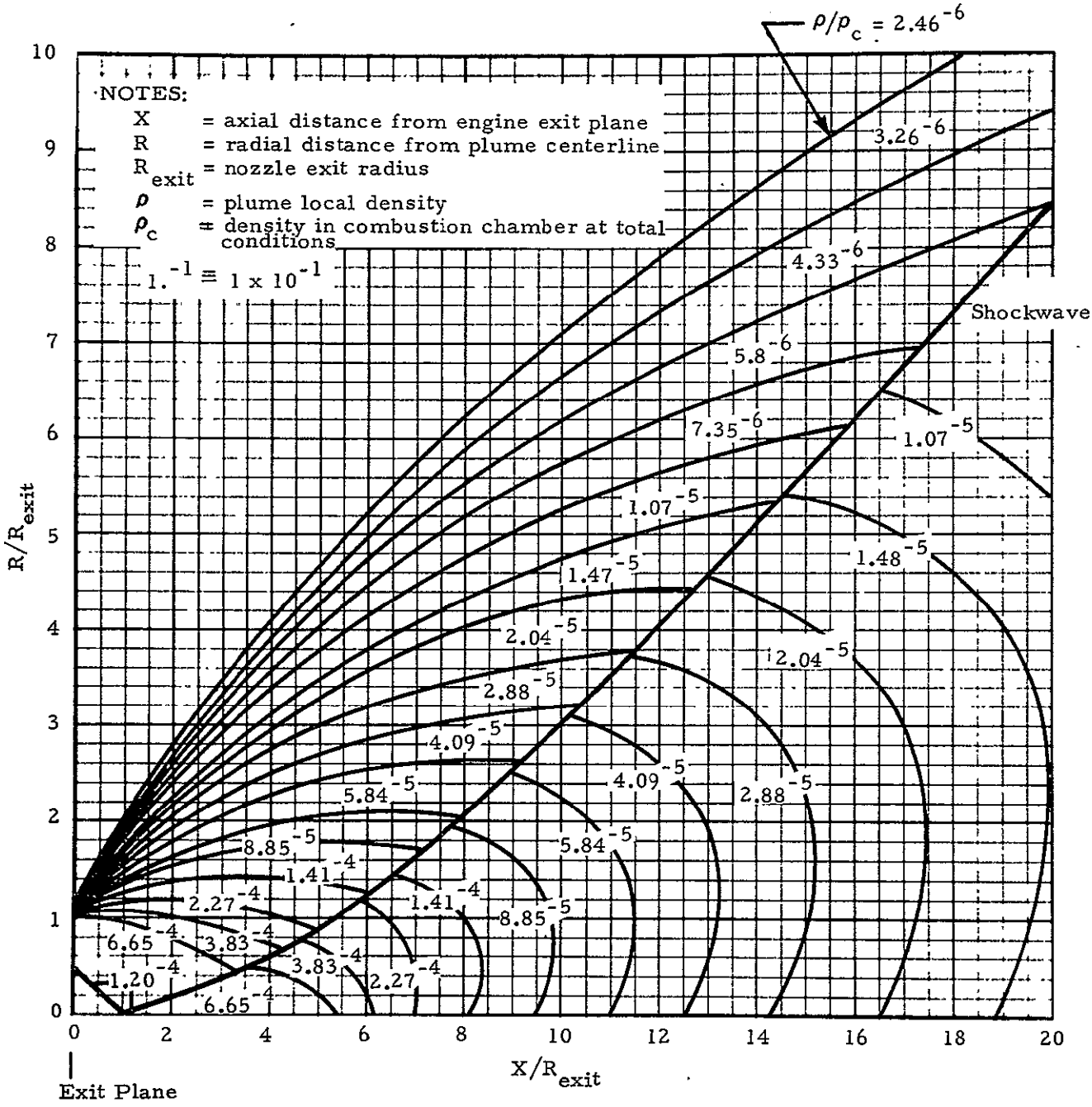

Fig. 5 - Local Density Contour Map for the Exhaust Plume Flow Field

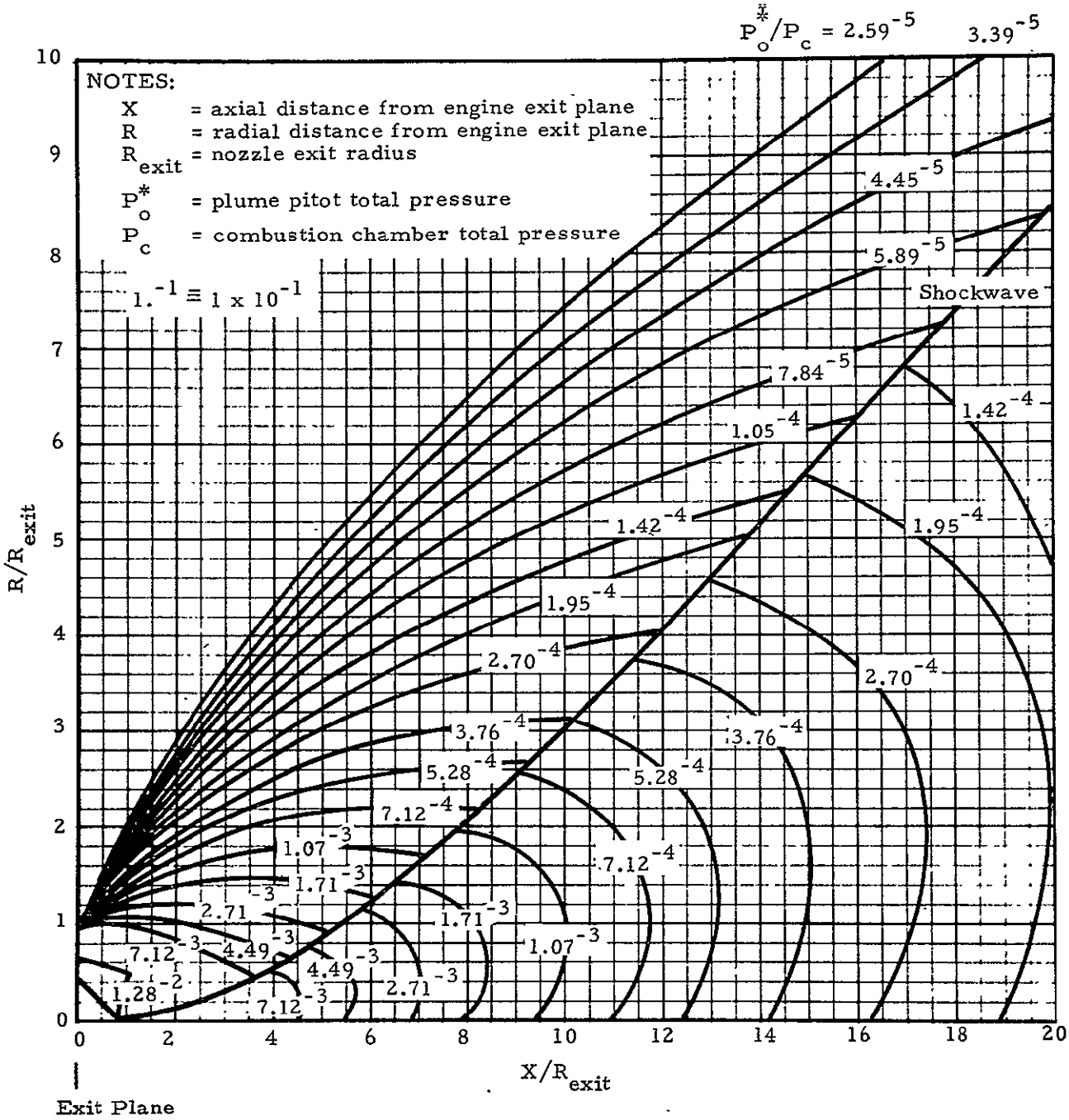

Fig. 6 - Local Pitot Total Pressure Contour Map for the Engine Exhaust Plume

Cylinder Test Model

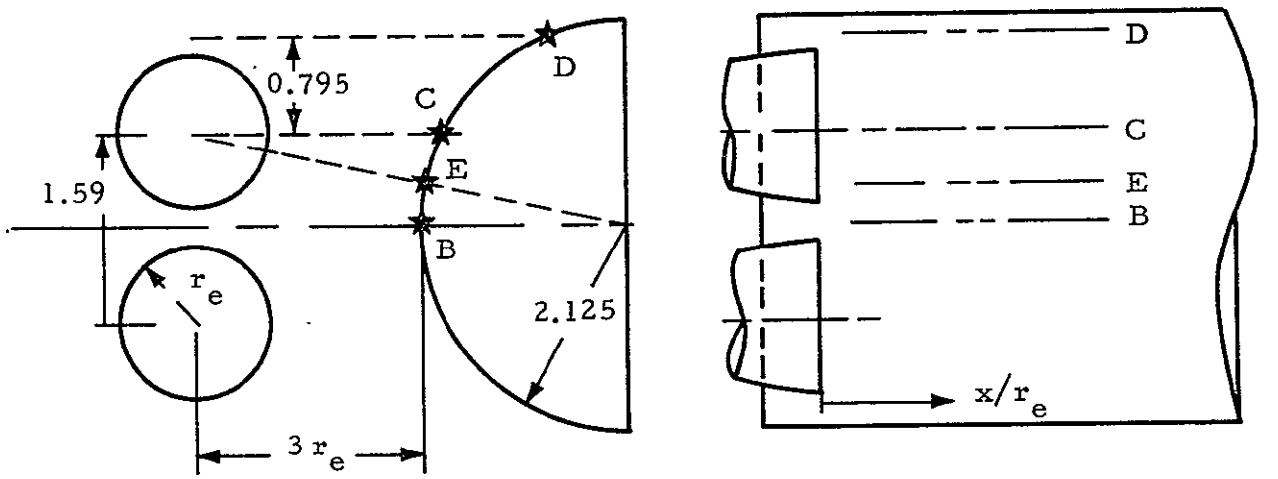

Note: Dimensions are in inches

Flat Plate Test Model

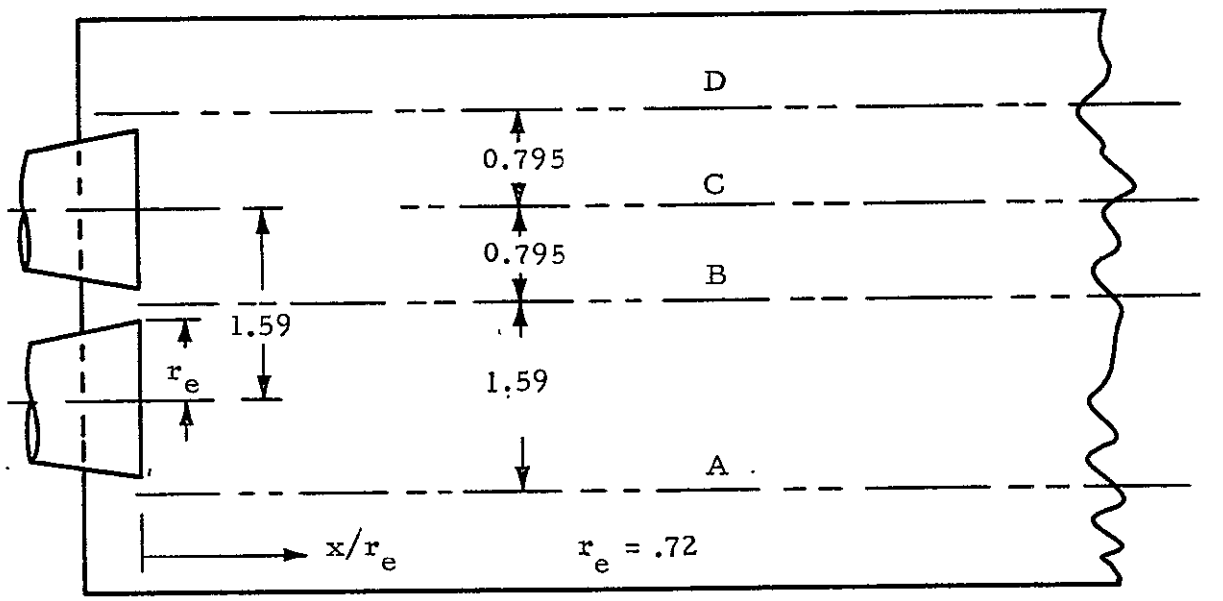

Fig. 7 - Sketch of Cylinder and Flat Plate Test Models

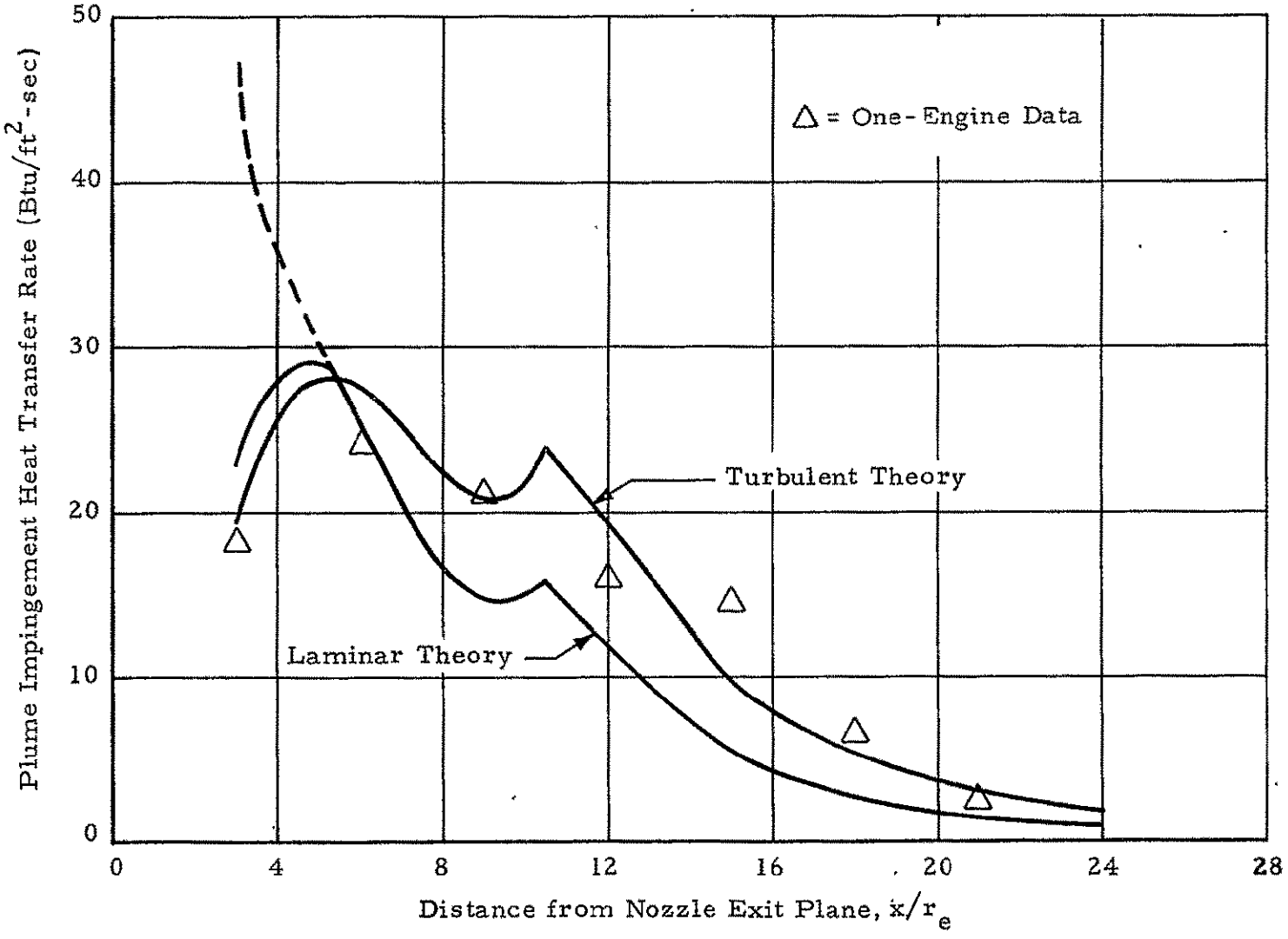

Fig. 8 - Flat Plate Heat Transfer Distribution on Centerline for Single Engine (Row C)

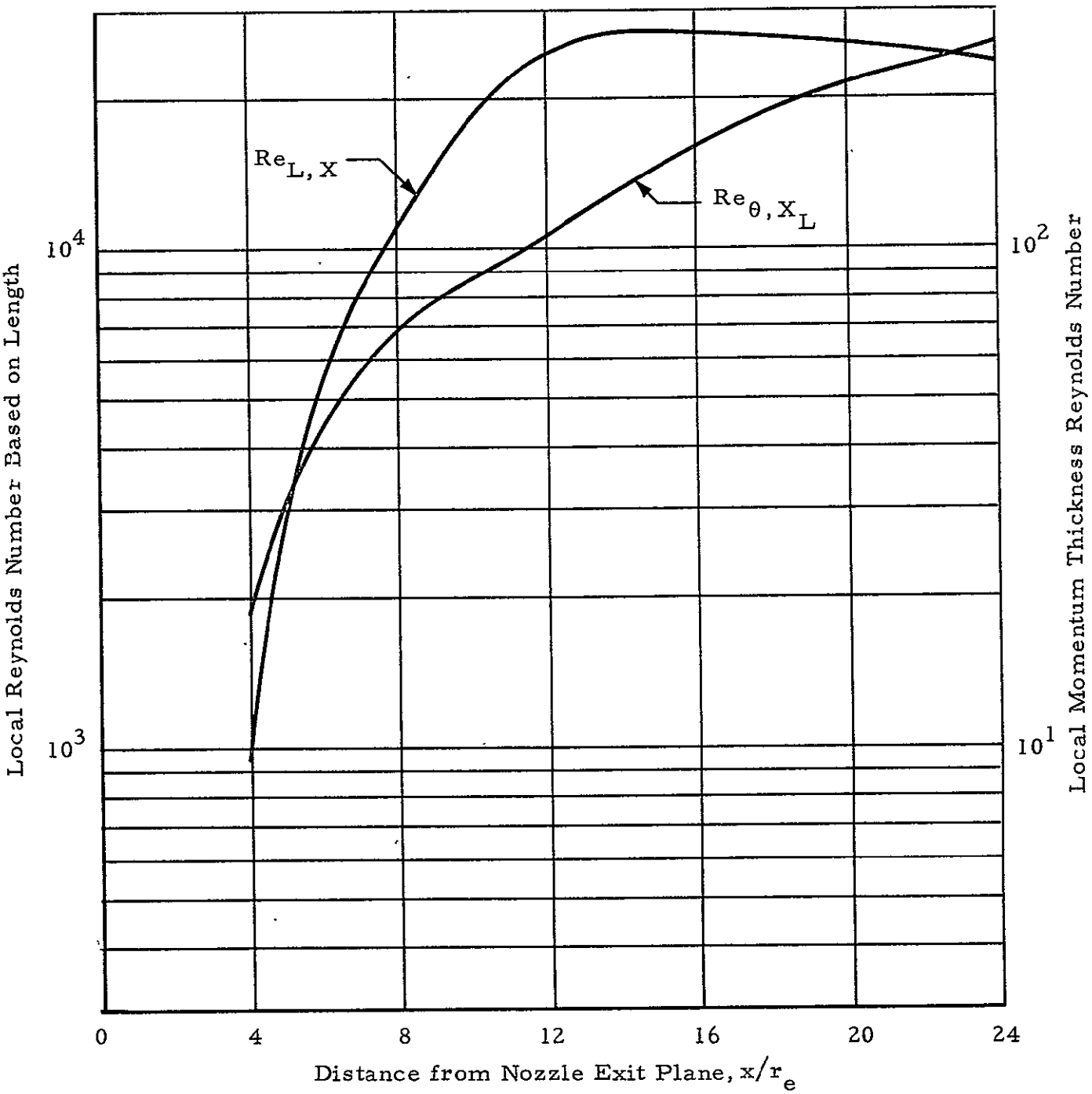

Fig. 9 - Flat Plate Local Reynolds Number and Momentum Thickness Reynolds Number Distribution for Single-Engine Firing (Row C)

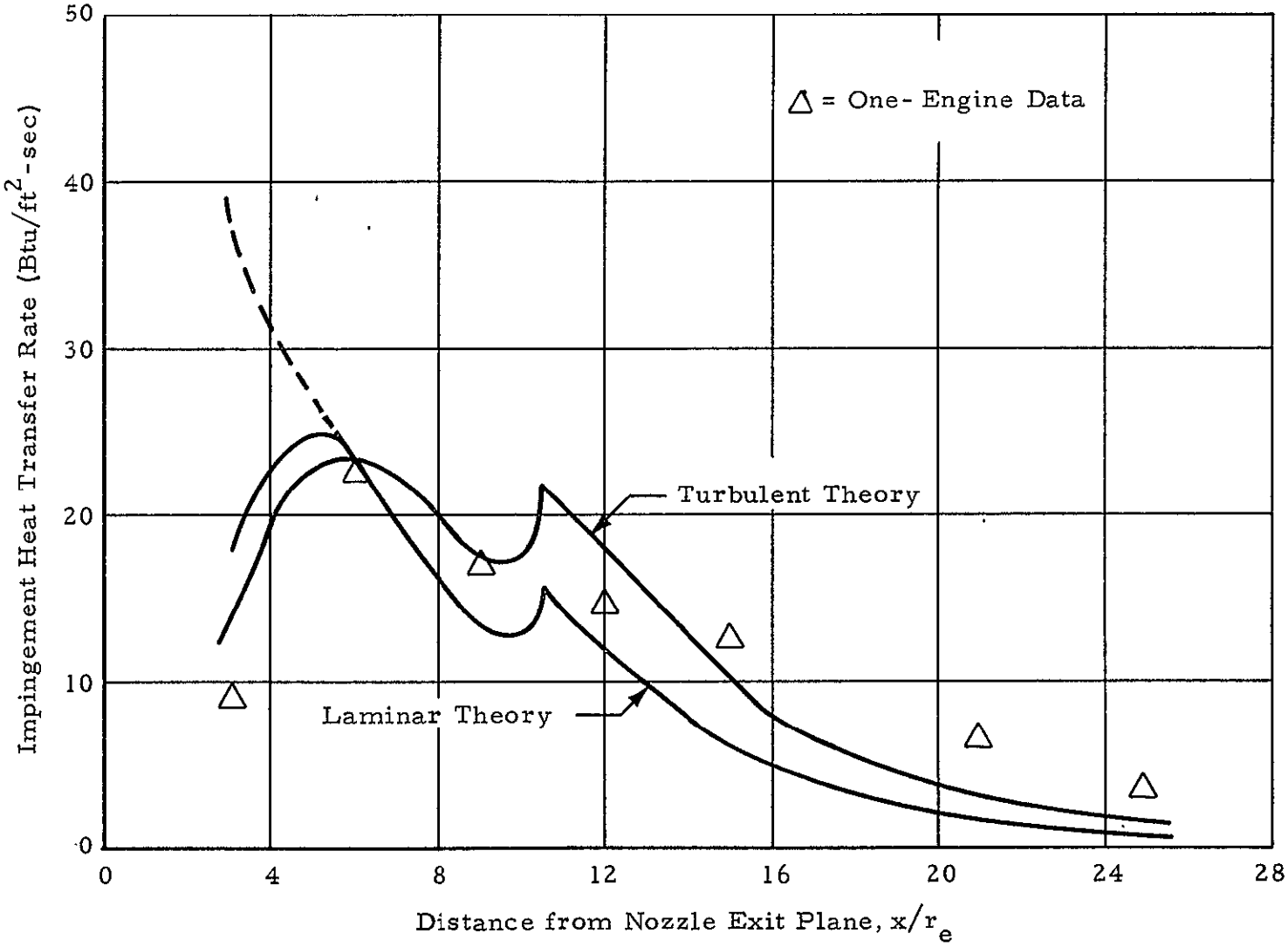

Fig. 10 - Flat Plate Heat Transfer Distribution on Body Centerline for Single Engine (Row

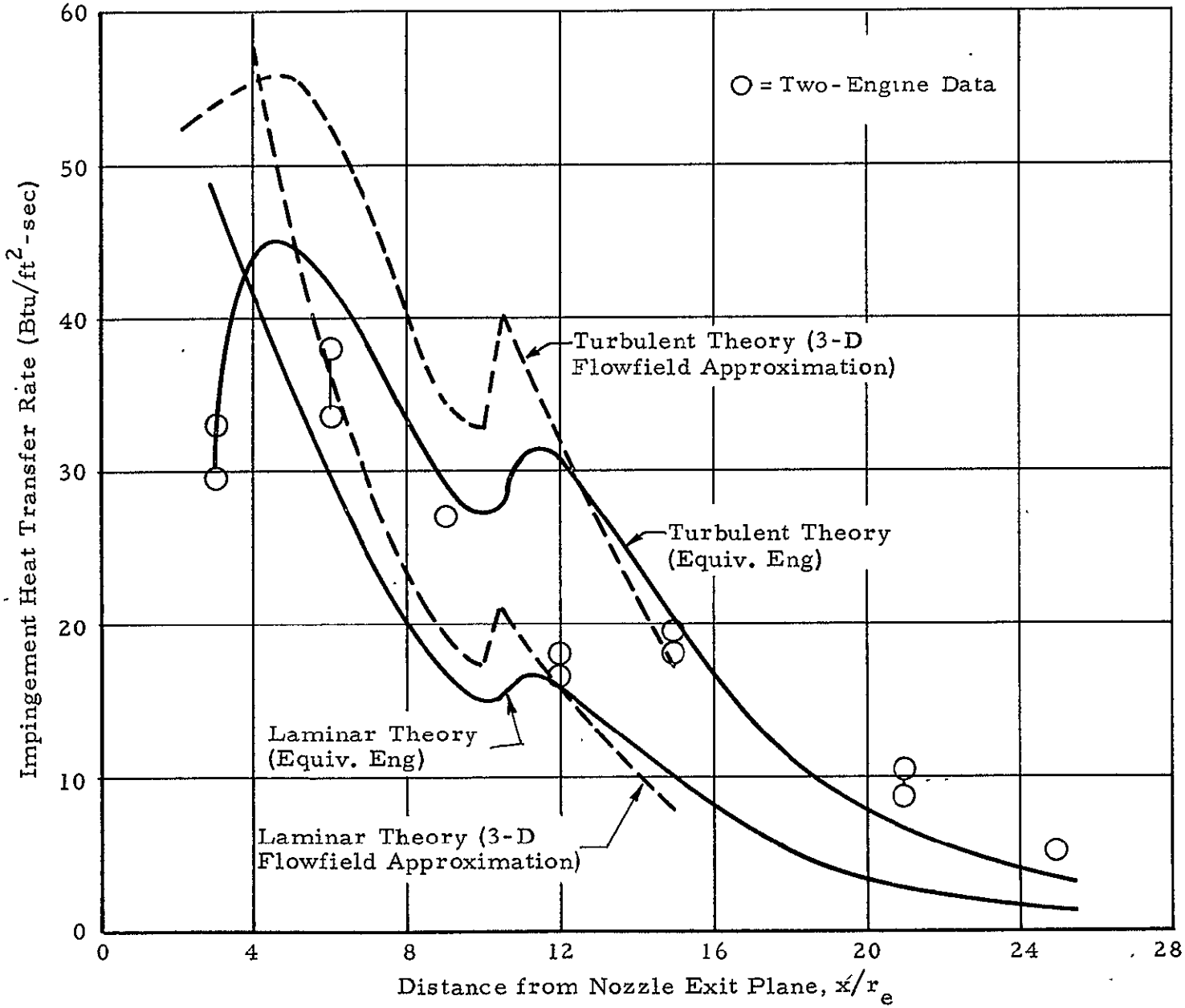

Fig. 11 - Flat Plate Heat Transfer Distribution on Body Centerline for Two Engines (Row B)

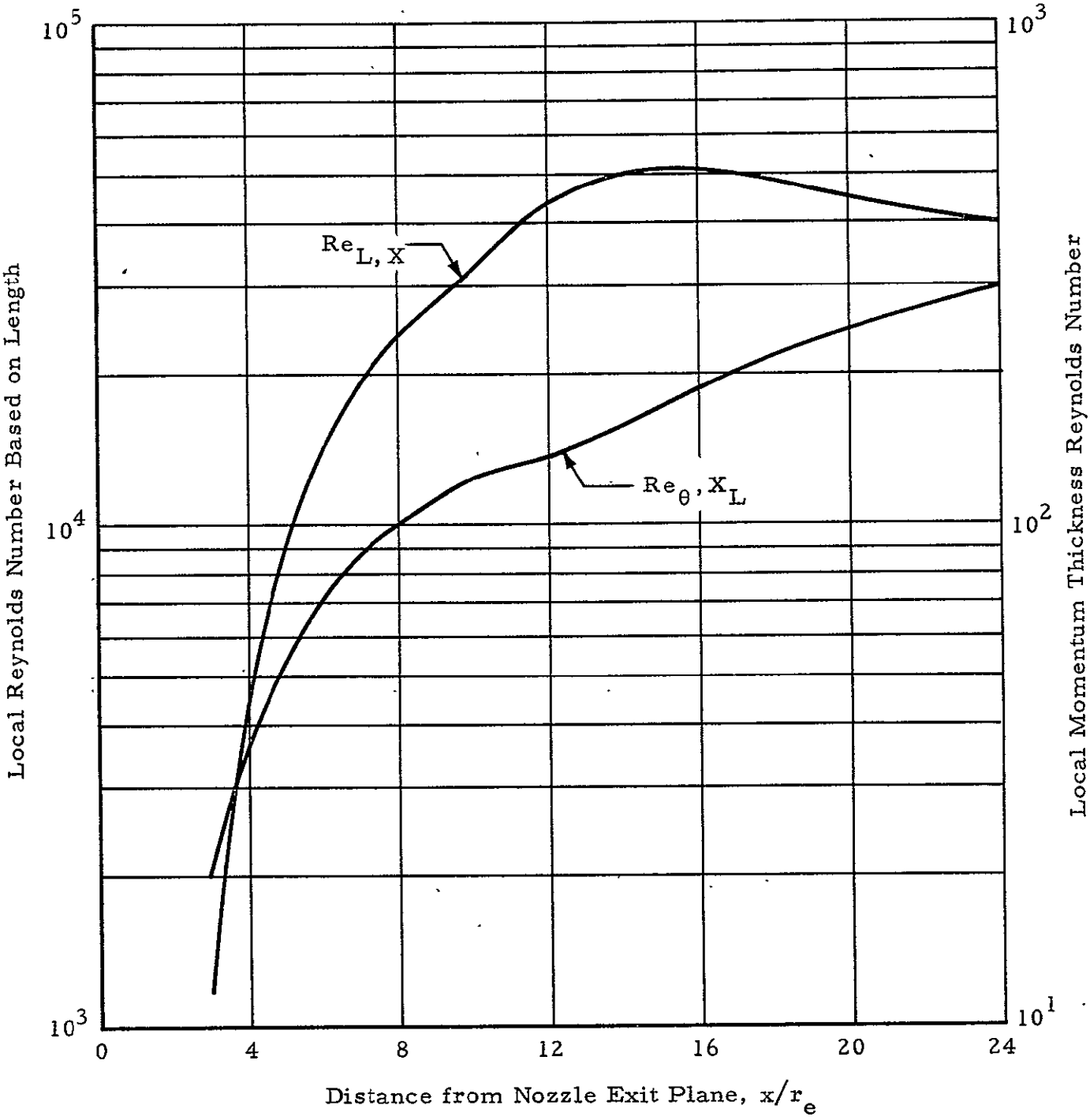

Fig. 12 - Flat Plate Local Reynolds Number and Momentum Thickness Reynolds Number Distribution for Two Engines Firing (Row B)

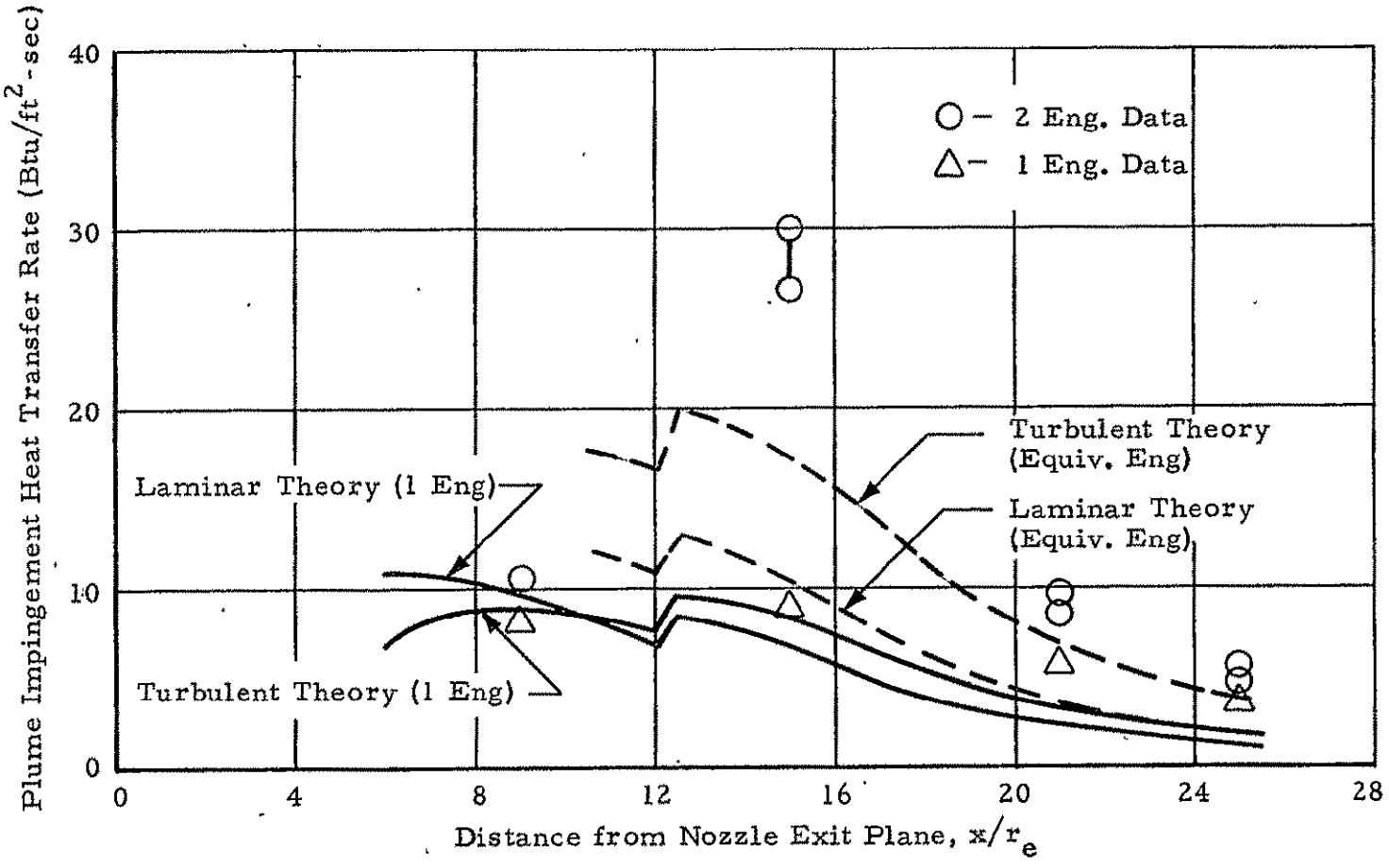

Fig. 13 - Flat Plate Heat Transfer Distribution (Row A)

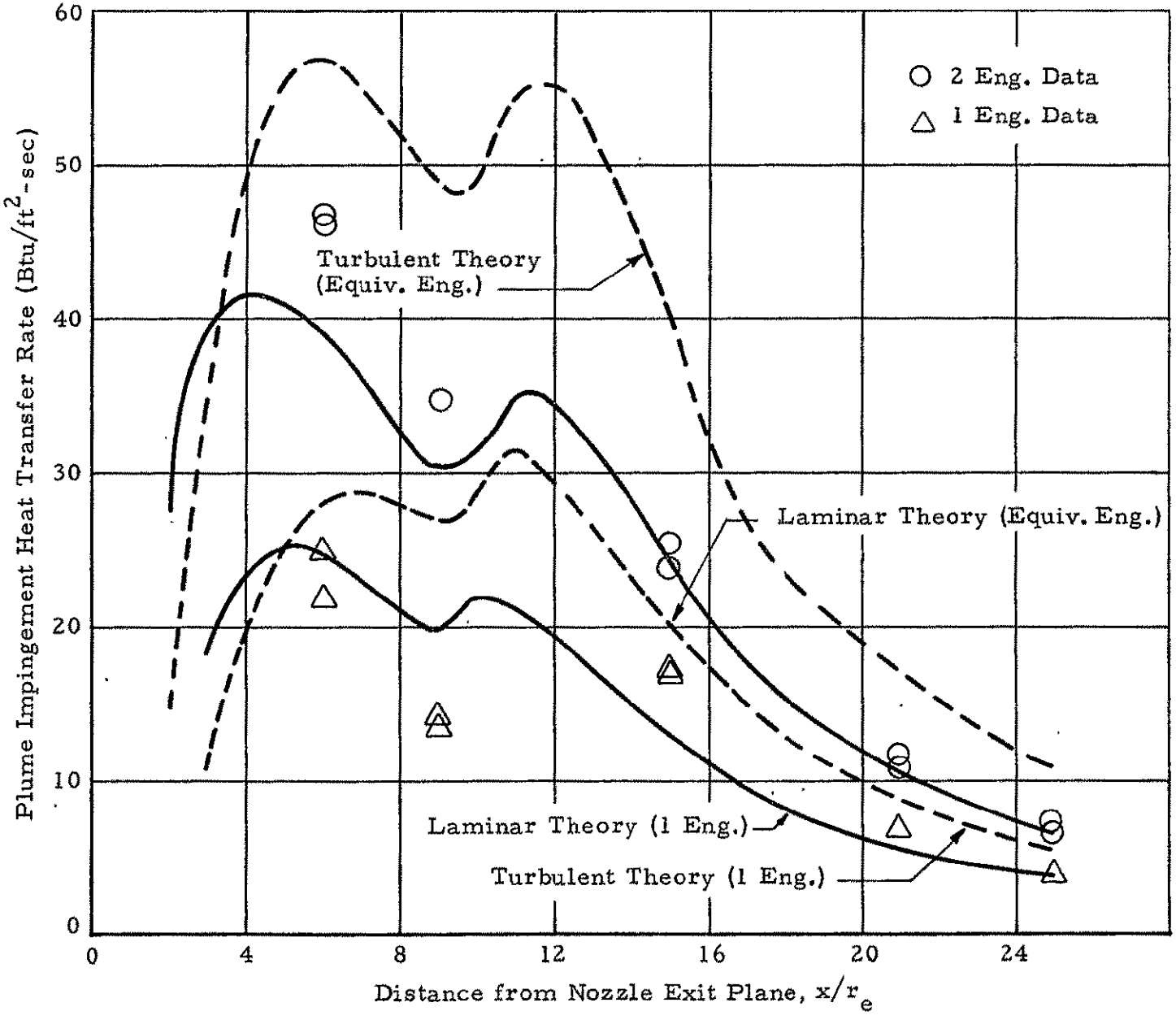

Fig. 14 - Cylinder Heat Transfer Rate Distribution on Body Centerline (Row B)

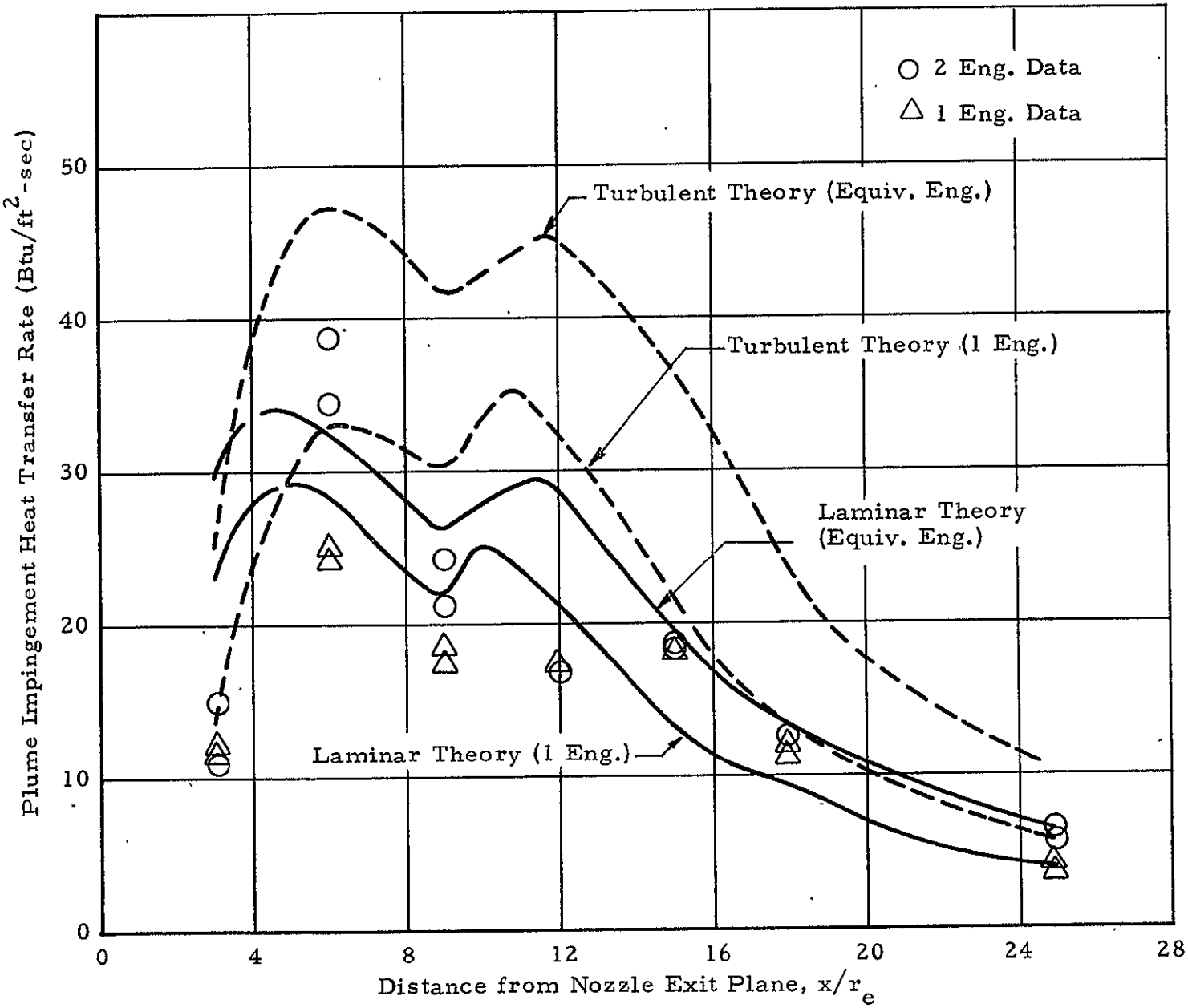

Fig. 15 - Cylinder Heat Transfer Distributions off Body Centerline (Row E)

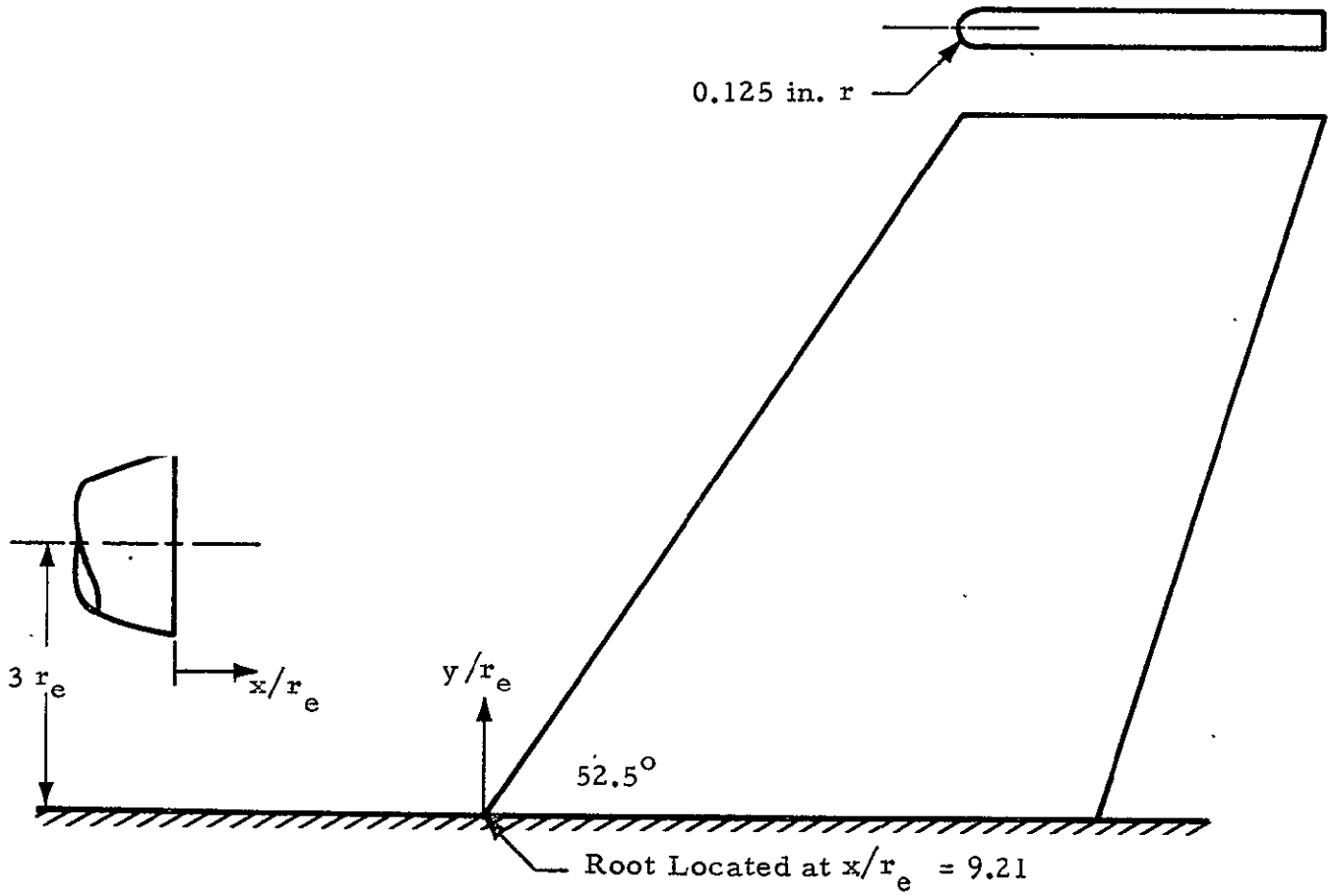

Fig. 16 - Sketch of GAC Vertical Fin Model

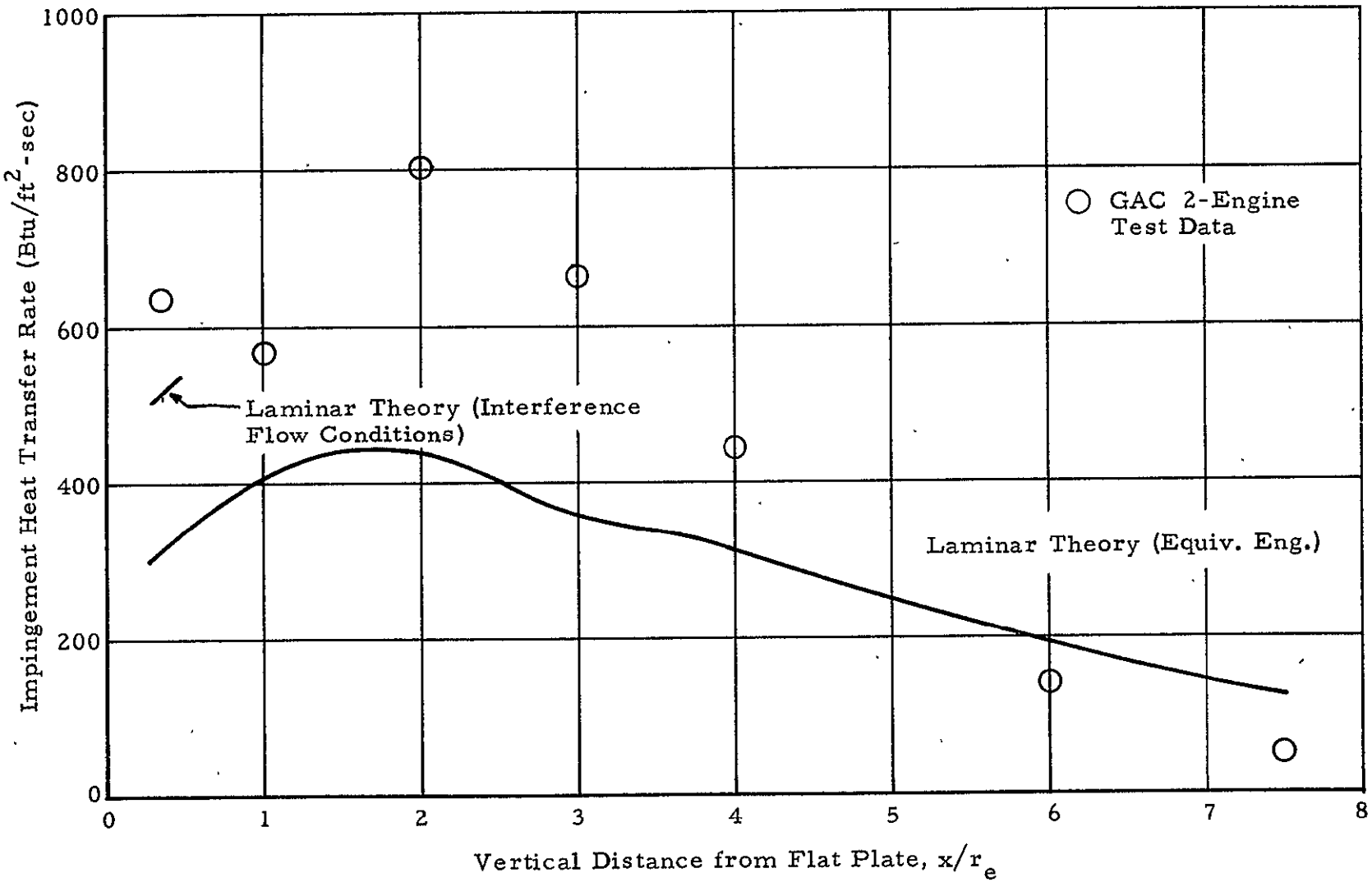

Fig. 17 - Fin Heat Transfer Distribution on Fin Leading Edge

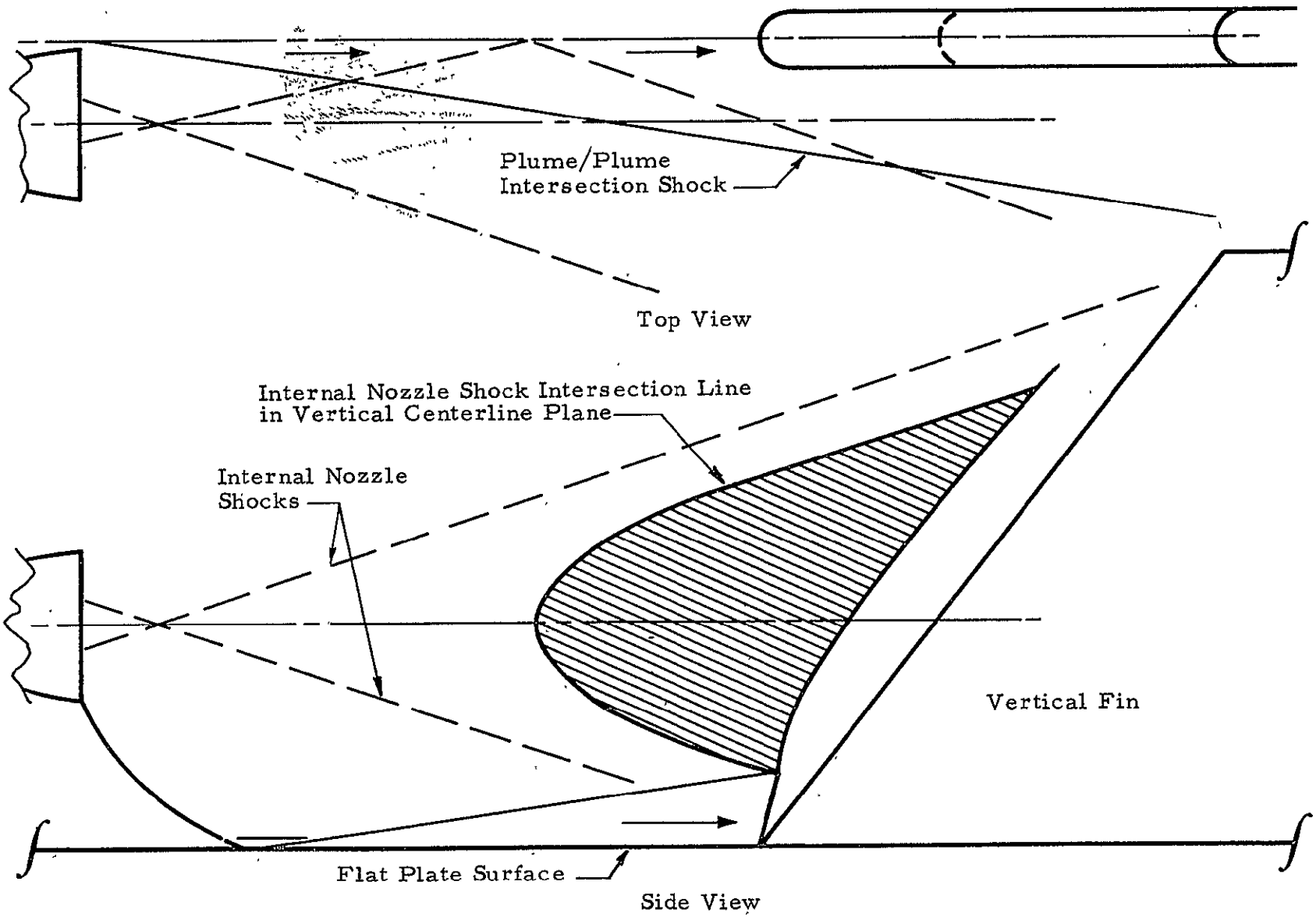

Fig. 18 - Sketch of Two-Engine Plume Shock Structure